JACS
JOURNAL OF THE AMERICAN CHEMICAL SOCIETY

Article

pubs.acs.org/JACS

Macroscopically Aligned Graphite Films Prepared from Iodine-Doped Stretchable Polyacetylene Films Using Morphology-Retaining Carbonization

Satoshi Matsushita and Kazuo Akagi*

Department of Polymer Chemistry, Kyoto University, Katsura, Kyoto 615-8510, Japan

Supporting Information

ABSTRACT: We prepared graphite films using typical Shirakawa-type and stretchable polyacetylene (PA) films as precursors through a morphology-retaining carbonization. A macroscopically aligned PA film was prepared from the drawable PA film using a mechanical-stretching procedure. The degree of orientation of the aligned PA film was evaluated by measuring polarized infrared absorption spectra and an azimuthal-angle profile of a Laue X-ray diffraction (XRD) pattern. The carbonization was performed from the iodine-doped PA films as precursors at 800 °C. The carbon films were subsequently graphitized at 1400−3000 °C, yielding graphite films with almost the same surface morphology as that of the original PA films and that of the carbon films as precursors. The typical PA film graphitized at 2600 °C exhibited tensile strengths of up to 224 MPa, moduli of up to 10 GPa, and an average electrical conductivity of 2.5×10^2 S/cm. In contrast, the graphite film prepared from the stretched PA film presented a Laue XRD pattern in which graphitic crystal structures are aligned parallel to the direction of stretching of the PA film. The anisotropic graphite film showed an enhanced conductivity of up to 1.5×10^3 S/cm along the stretching direction. We demonstrated that an iodine-doped PA film is a highly efficient carbon source for producing graphite films with good mechanical and electrical properties. The total yield of a graphite film is as high as 61−74% at up to 3000 °C, which is considerably higher than that of polyacrylonitrile-based carbon fiber and polyimide-based graphite film.

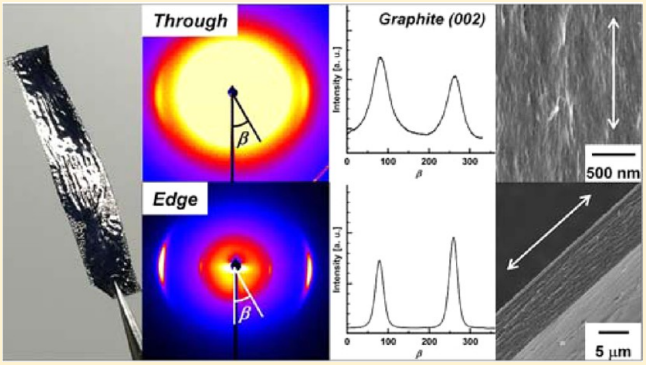

1. INTRODUCTION

Carbon-based freestanding films, such as graphite foils,[1] carbon nanotube (CNT) buckypapers,[2] and graphene-based papers,[3] have recently attracted considerable attention because of their high mechanical flexibility, electrical properties, and excellent chemical and thermal stabilities. Therefore, these films are currently being used in industrial applications in various fields. Graphite foils are generally fabricated by rolling thermally expanded graphite flakes. In contrast, CNT- and graphene-based papers are often fabricated from dispersed CNTs and chemically exfoliated graphenes using a solution processing route with a vacuum filtration technique. The chemical vapor deposition growth method is also widely employed as a direct fabrication technique for freestanding CNT films.[4] A number of approaches have been reported for efficiently preparing high-quality and large-scale carbon-based films that exhibit exceptional performance. However, fabricating carbon materials with desirable forms, such as nanofibers, anisotropic structures, and hierarchical structures, is generally difficult. For potential advanced applications of carbon-based films, particularly in the fields of nanotechnology and carbon electronics, precise morphology control based on a bottom-up approach is a key factor.[5,6]

We have recently succeeded in preparing hierarchical helical graphite films through a solid-state carbonization and a subsequent graphitization, in which graphitic carbon fibrils are helically bundled and spirally arranged.[7] These helical graphite films were prepared from helical aliphatic and aromatic conjugated polymer films, such as iodine-doped helical polyacetylene (PA) and ClO_4^--doped helical poly(3,4-ethylenedioxythiophene) films, as carbonization precursors that are synthesized through a chemical or electrochemical polymerization in a chiral nematic liquid crystal as an asymmetric reaction field. Notably, the novel carbonization method provides stable freestanding graphite films from unstable aliphatic conjugated polymer films. The iodine doping is the most important and indispensable procedure for preventing thermal decomposition and for retaining the morphology of the PA precursor film. Because PA has a high carbon content (~92.3%), the theoretical carbonization yield after the heat treatment is supposed to be higher than that of other precursor polymers, such as polyacrylonitrile (PAN, ~67.9%) and polyimide (PI, ~67.4%), which are representative carbonization precursors for the production of carbon fibers[8] and graphite

Received: April 18, 2015
Published: June 23, 2015

DOI: 10.1021/jacs.5b04012
J. Am. Chem. Soc. 2015, 137, 9077−9087

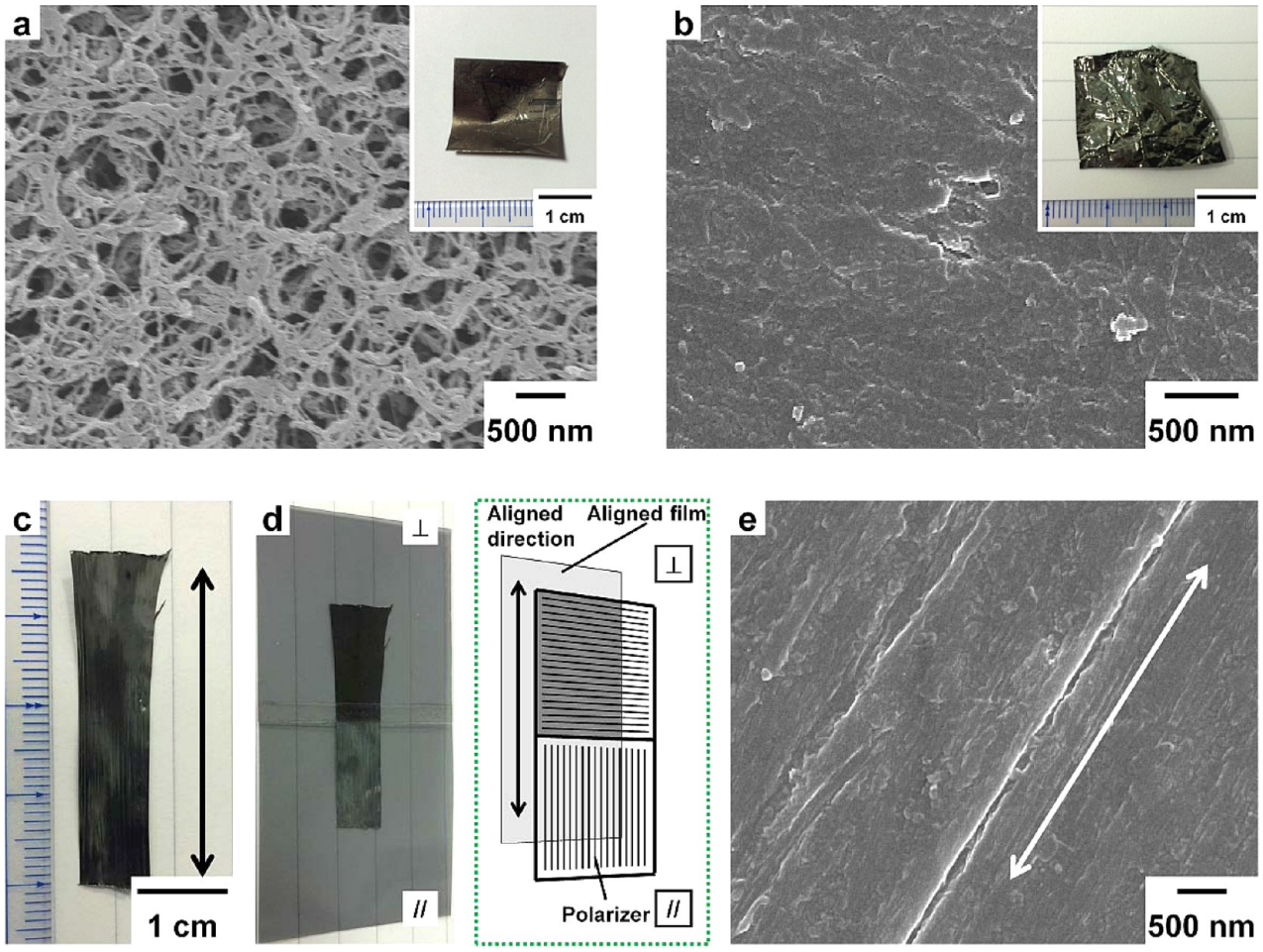

Figure 1. SEM images of the (a) S-type (gas side), (b) unstretched (as-polymerized), and (e) mechanically stretched PA films. The insets present photographs of the (a) S-type [gas side, thickness (t) = 107 ± 2 μm, bulk density (d_{bulk}) = 0.72 g/cm^3] and (b) unstretched (t = 26 ± 4 μm, d_{bulk} = 1.16 g/cm^3) PA films. Photographs of the (c) stretched [draw ratio (l/l_0) ca. 4] PA film and the (d) film in which two polarizers are arranged parallel (bright) and perpendicular (dark) to the direction of stretching of the PA film. A schematic illustration is also presented in part d. These samples are pristine PA films before the iodine doping.

films,[9] respectively. Indeed, previous studies reported that the novel carbonization procedure affords a high carbonization yield of approximately 80% at 800 °C.[7a,b] Although helical graphite films are anticipated to be used in potential applications based on their helical structure and electrical conductivity, such as graphene aggregates, carbon electrodes, and molecular magnets based on an induced solenoid magnetism, their intrinsic performance is still too low for use in such applications, even in a macroscopically aligned helical graphite film,[7b] when compared with the theoretical properties of a natural graphite single crystal, a single-layer graphene sheet, and the above-described carbon-based papers. Therefore, improving the mechanical and electrical properties of graphitic materials produced from conjugated polymeric precursors is of considerable importance.

One of the most promising approaches for enhancing the electrical conductivity of graphite films is the macroscopic alignment of polymer films used as precursors.[10] The direct synthesis of a macroscopically aligned PA film has previously been successfully achieved using a highly oriented nematic liquid crystal with a monodomain structure through a gravity-flow technique,[11] a magnetic field method,[12] or a combination of the two methods.[13] The PA film with a highly aligned fibril morphology exhibited a distinct enhancement in its anisotropic electrical conductivity. The order parameter of the aligned PA film has been reported to be approximately equal to the value for nematic liquid crystals. In other words, the order parameter of the PA film has never exceeded that of the nematic liquid crystal as long as the liquid-crystal polymerization method is used to synthesize the aligned PA film. By contrast, highly stretchable PA films with high tensile properties have been synthesized through using the method of Naarmann and Theophilou,[14] a solvent evacuation method,[15] and an intrinsic nonsolvent method.[16] The conductivity of the PA film was enhanced through a uniaxial alignment of the polymer chains, which was associated with the mechanical stretching of the film following polymerization. In these methods, the high-temperature-aged catalyst solution affords PA film with high density and mechanical stretchability. Indeed, among conjugated polymers, the highest electrical conductivity has been reported in a mechanically aligned PA film doped with iodine.[17] If the highly stretched PA film is used as a carbonization precursor polymer, the production of an anisotropic graphite film with improved electrical conductivity might be achieved.

In this study, first we present (i) freestanding graphite films with an entangled fibril morphology that were prepared from iodine-doped typical Shirakawa-type (S-type) PA films[18] through a morphology-retaining carbonization method and a

DOI: 10.1021/jacs.5b04012
J. Am. Chem. Soc. 2015, 137, 9077−9087

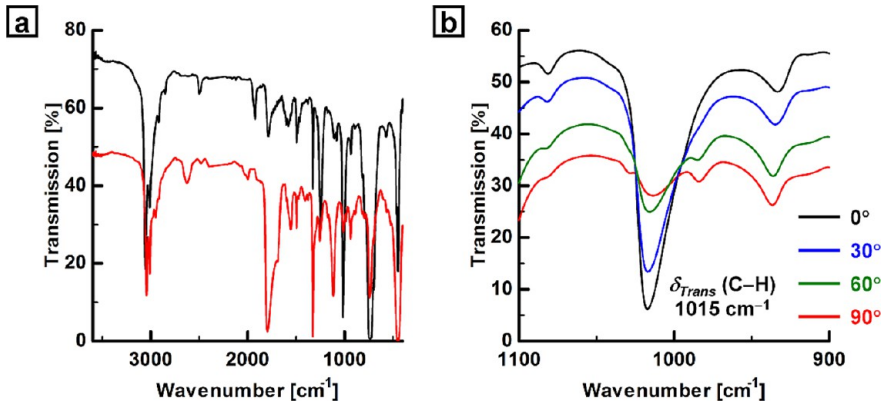

Figure 2. (a) Polarized IR absorption spectra of the stretched PA film and (b) their magnified spectra.

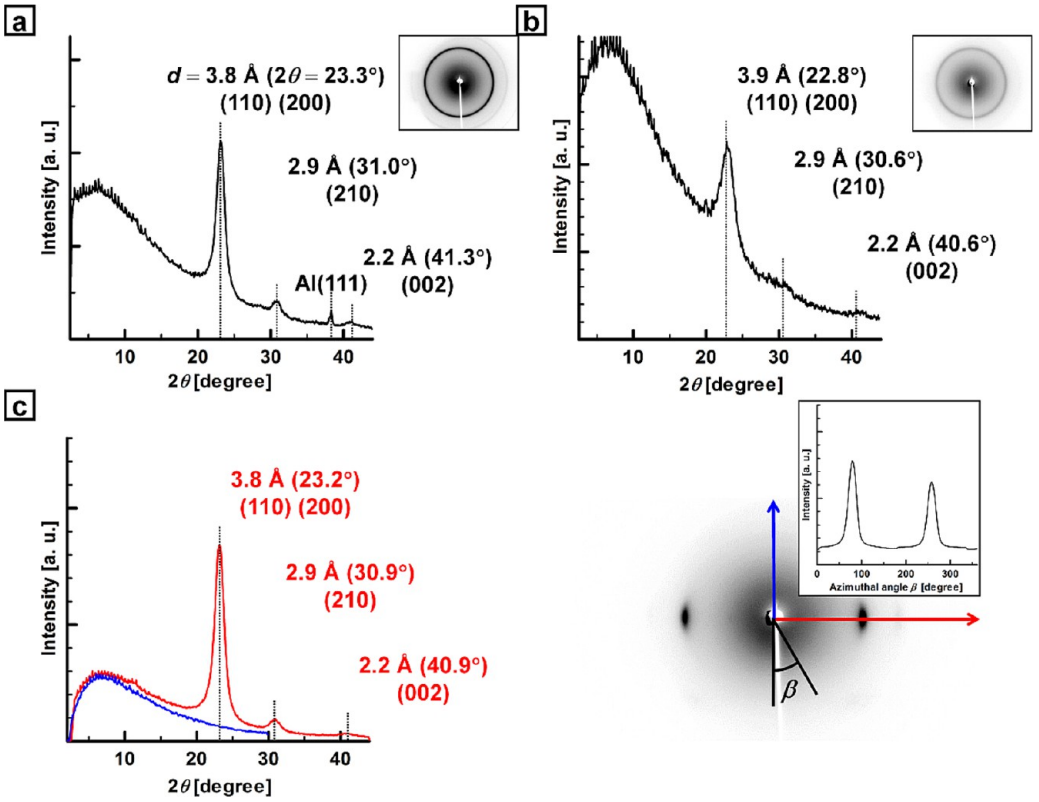

Figure 3. XRD patterns of the (a) S-type, (b) unstretched (as-polymerized), and (c) mechanically stretched (l/l_0 ca. 4) PA films. The incident X-rays are perpendicular to the film surface. The inset shows the azimuthal-angle profile based on the (110) and (200) reflections of the XRD pattern. These samples are pristine PA films before the iodine doping.

subsequent graphitization procedure at very high temperatures of up to 3000 °C. The carbonization and graphitization procedures were optimized to achieve high crystallinity and electrical conductivity in the obtained graphite film. Next, we present (ii) macroscopically aligned graphite films that were prepared from highly stretched PA films using the optimized heat-treatment condition. The aligned PA film was prepared by drawing the stretchable PA film synthesized using the solvent evacuation method.

2. RESULTS AND DISCUSSION

2.1. Morphologies of PA Films. The S-type and stretchable PA films were synthesized through an interfacial acetylene polymerization in isotropic solvents, such as toluene and cumene, using the Ziegler–Natta catalyst *tetra-n*-butoxytitanium [Ti(O-*n*-Bu)$_4$] and triethylaluminum (AlEt$_3$). The full experimental details of the polymerization methods are described in the Supporting Information. Figure 1 presents photographs of the S-type, unstretched (as-polymerized), and mechanically stretched PA films with a metallic luster. The glass and gas sides of the typical PA film exhibited shiny and dull metallic lusters, respectively. The stretchable PA film could be drawn approximately four times in length without breaking under nitrogen gas at room temperature. This film also exhibited a linearly polarized dichroism when the polarizer was arranged parallel (bright) or perpendicular (dark) to the stretching direction of the film (Figure 1d). In contrast, the typical PA film only exhibited a weak stretchability at room temperature.[19] Figure 1a presents a scanning electron microscope (SEM) image of the typical PA film. This image shows

DOI: 10.1021/jacs.5b04012
J. Am. Chem. Soc. 2015, 137, 9077–9087

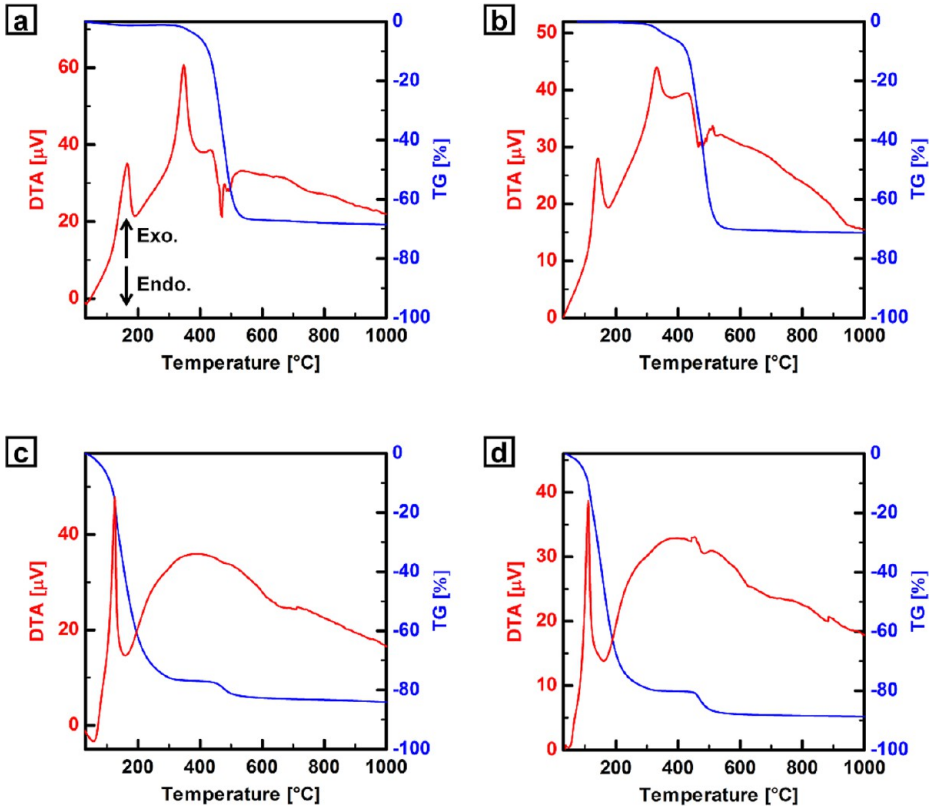

Figure 4. TG-DTA curves of the (a) pristine S-type, (b) pristine stretchable, (c) iodine-doped S-type ($[CHI_{0.35}]_n$), and (d) iodine-doped stretchable ($[CHI_{0.42}]_n$) PA films.

that a number of fibrils with thicknesses of less than 100 nm are entangled. By contrast, the stretchable PA film shows no clear fibril morphology, regardless of whether the PA film is in a mechanically stretched state (Figure 1c,e). As observed from the SEM image of the stretched PA film, the polymer chains are macroscopically aligned parallel to the direction of mechanical stretching.

2.2. Polarized IR Absorption Spectra of PA Films. Infrared (IR) absorption spectra of the PA films were measured. The *cis* contents were determined from the absorption bands at 740 and 1015 cm^{-1} attributed to *cis* and *trans* C−H out-of-plane vibrations, respectively. The present S-type and stretchable PA films have a high *cis* content of 87% (Figure S1 in the Supporting Information), which is due to the low polymerization temperature of −78 °C. Subsequently, the polarized IR absorption spectra parallel (0°) and perpendicular (90°) to the stretching direction of the mechanically drawn PA film were measured (Figure 2). The IR dichroic ratio (R) and the optical order parameter (S) of the stretched PA film were determined to be 10.8 and 0.76, respectively, where R is defined as $R = A_{1015,\parallel}/A_{1015,\perp}$ and S is defined as $S = (R - 1)/(R + 2)$.[20] Here, $A_{1015,\parallel}$ and $A_{1015,\perp}$ represent the integrated absorbances of polarized light at 1015 cm^{-1} parallel and perpendicular to the aligned direction of the film, respectively. The present optical anisotropy and the relatively high order parameter indicate a significant alignment of PA chains along the direction of stretching. The orientational angle (θ), defined as $\theta = \cos^{-1}[(2R - 1)/(2R + 1)]^{1/2}$, was calculated to be 17°.[21]

2.3. XRD Patterns of PA Films. Figure 3a presents an X-ray diffraction (XRD) pattern of the typical PA film. The XRD pattern shows sharp (110) and (200) reflections at 3.8 Å (23.3° in 2θ), a small (210) reflection at 2.9 Å (31.0° in 2θ), and a (002) reflection at 2.2 Å (41.3° in 2θ). This result indicates that the typical PA film has a highly crystalline region inside the fibril.[11b] Figure 3b presents an XRD pattern of the unstretched PA film. The pattern shows (110) and (200) reflections at 3.9 Å (22.8° in 2θ), a (210) reflection at 2.9 Å (30.6° in 2θ), and a (002) reflection at 2.2 Å (40.6° in 2θ). Figure 3c presents an XRD pattern of the stretched PA film. The pattern shows sharp (110) and (200) reflections at 3.8 Å (23.2° in 2θ), a small (210) reflection at 2.9 Å (30.9° in 2θ), and a (002) reflection at 2.2 Å (40.9° in 2θ). As shown in Figure 3c, the fiber diagram in the pattern indicates a uniaxial alignment of the PA chains, which is in stark contrast to the Debye−Scherrer ring observed in XRD patterns of the S-type and unstretched PA films. The degree of orientation of the stretched PA film was estimated using Hermans' (second-order) orientation factor (f) based on the (110) and (200) reflections of the pattern using the equation $f = (\langle 3\cos^2 \varphi \rangle - 1)/2$, where φ is the peak width at half-maximum for the azimuthal-angle profile.[22] Consequently, the orientation factor was calculated to be as high as 0.81−0.82. From these results, the stretched PA films are anticipated to afford potential carbonization precursors consisting of inter-chain π-stacked polyene chains with uniaxially aligned structures.

2.4. TG-DTA Curves of PA Films. The thermal behavior of the undoped PA film in a heating run was compared with that of the iodine-doped film using thermogravimetric−differential thermal analysis (TG−DTA) up to 1000 °C (Figure 4). The DTA curve of the undoped typical PA film presented exothermic peaks at 165 and 347 °C and an endothermic peak in the range of 400−600 °C. These peaks are attributed to a *cis*−*trans* isomerization, a cross-linking, and thermal decomposition, respectively.[23] The decomposition is accom-

DOI: 10.1021/jacs.5b04012
J. Am. Chem. Soc. 2015, 137, 9077−9087

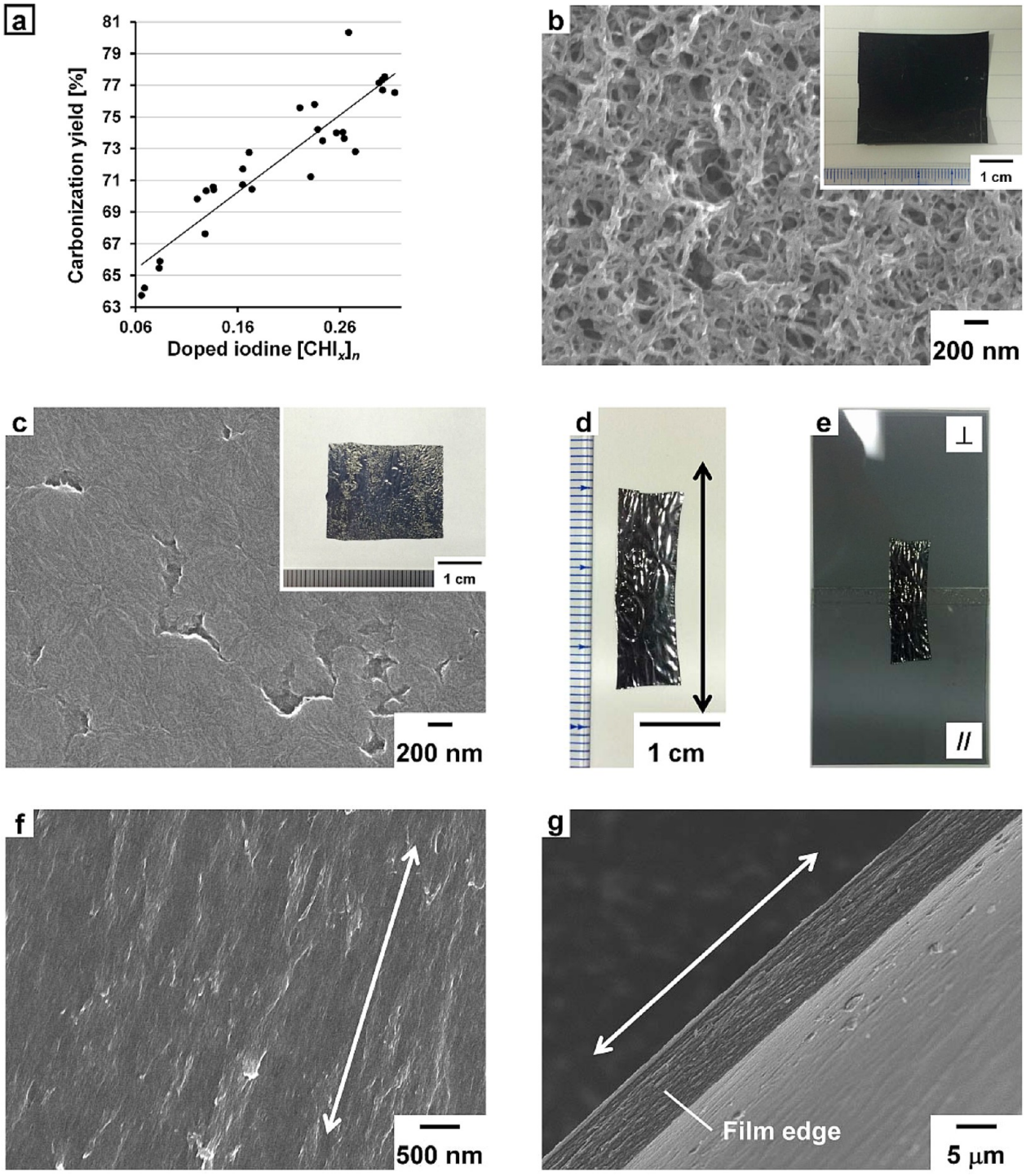

Figure 5. (a) Carbonization yield of the typical PA film as a function of the amount of doped iodine. SEM images of the (b) S-type (gas side), (c) unstretched, and (f, g) mechanically stretched PA films ($[CHI_{0.26-0.34}]_n$) graphitized at 2600 °C. The insets show photographs of the (b) S-type [precursor, $[CHI_{0.27}]_n$, gas side; t = 55 ± 6 μm, d_{bulk} = 1.32 g/cm^3, electrical conductivity (σ) = 257 ± 22 S/cm] and (c) unstretched ($[CHI_{0.26}]_n$, t = 46 ± 8 μm, d_{bulk} = 1.05 g/cm^3, σ = 282 ± 33 S/cm) PA films graphitized at 2600 °C. Photographs of the (d) stretched PA film ($[CHI_{0.34}]_n$, t = 14 ± 0 μm, d_{bulk} = 1.61 g/cm^3, $\sigma_{\|}$ 539 ± 39 S/cm) graphitized at 2600 °C and the (e) aligned graphite film with polarizers.

panied by a large weight loss (67% at 600 °C) of the PA film due to the volatilization of hydrocarbon gases, such as benzene, toluene, methane, and ethylene,[24] as shown in the TG curve (Figure 4a). The DTA curve of the stretchable PA film reveals that polyene chains are transformed from a *cis* form to a *trans* form at 142 °C, are cross-linked at 331 °C, and are thermally decomposed in the range of 400−600 °C (Figure 4b). In contrast, in the case of the doped PA film, the DTA curve shows that a transformation from *cis* form to *trans* form occurs at 111−125 °C, after which the weight of the film rapidly decreases as the temperature increases up to 300 °C due to an evaporation of excess doped iodine. Furthermore, a small decrease in weight is observed in the range of 400−500 °C. The doped PA film showed no endothermic peaks attributed to

DOI: 10.1021/jacs.5b04012
J. Am. Chem. Soc. 2015, 137, 9077−9087

thermal decomposition in the DTA curves (Figure 4c,d). The thermal behavior of these S-type and stretchable PA films is similar to that of aligned and helical PA films synthesized in a liquid-crystal reaction field.[7a,b]

Here, it is of interest to discuss the role of iodine in PA films during the heat treatment. From the TG−DTA results, it is clear that the doped iodine prevents the PA film from undergoing a thermal decomposition during the heat treatment. In our previous work, a plausible mechanism of the preparation of carbon films from iodine-doped PA films was suggested: the iodine dopant reacts with the hydrogen atoms in the polymer chain, leading to the formation of hydrogen iodide gas during the heat treatment, and the polymer chains partially cross-link between the adjacent chains. Consequently, it is possible to prepare carbon and graphite films with completely preserved morphologies and even fibril structures. Further details about the mechanism are presented in the previous literature.[7a,b] The carbon and graphite films with retained morphology are presented in section 2.6.

2.5. Iodine Doping, Carbonization, and Graphitization of PA Films. Iodine doping was performed by exposing the PA film to iodine gas at room temperature for 2−186 h in a glass vial. The iodine doping of the stretchable PA film was performed after the mechanical stretching treatment of the PA film. The amount of iodine doped into the films was determined by weighing the doped PA films. The atomic ratio of doped iodine to carbon in the PA film (I/C) was 0.07−0.36. The doped PA film was placed between carbon plates (80 × 80 × 2−10 mm) and was inserted into an electric furnace. The doped PA film was then carbonized at 800 °C in the electric furnace for 1 h under flowing argon gas. The heating rate was 10 °C/min. The yields of the carbon films after the carbonization of the S-type and stretchable PA films were as high as 64−80 and 62−74% of the weight of the PA film prior to iodine doping, respectively. Note that the carbonization yield was determined using the equation

$$100[(\text{weight of carbonized PA film})/(\text{weight of PA film})]$$

The "weight of PA film" means a pristine PA film before the iodine doping. The degree of shrinkage of the typical PA film ($[CHI_{0.26}]_n$) during the carbonization was 66% of the area of the film prior to iodine doping. The carbonization yield of the typical PA film increased as the amount of doped iodine increased (Figure 5a). The elemental analysis (EA) results for carbonized typical PA film ($[CHI_{0.26}]_n$) are as follows: C, 94.43; H, 0.71; N, 0.16; and O, 2.08 (total, 97.38%). On the basis of the EA results, no iodine was detected in the carbon film. The EA results for the carbon film prepared from the stretchable PA film ($[CHI_{0.26}]_n$) are as follows: C, 96.65; H, 0.64; N, 0.54; and O, 0 (total, 97.83%).[25] The carbonized film was further heated at 1400−3000 °C with a graphitizing apparatus under flowing argon gas. The graphitization time was 30 min for 1400−2600 °C and 1 min for 3000 °C. The graphitization yields of the S-type and stretchable PA films graphitized at 2600 °C were 89−96 and 91−97%, respectively. The EA results for the typical PA film ($[CHI_{0.13}]_n$) graphitized at 2600 °C were as follows: C, 99.80 and H, 0. Note that the carbon films that were heat-treated at temperatures above 1400 °C possessed a carbon content of ∼100% (precursor, $[CHI_{0.24}]_n$; temp, 1400 °C; EA: C, 99.35 and H, 0). In contrast, the EA results for the stretchable PA film ($[CHI_{0.08}]_n$) graphitized at 2600 °C were as follows: C, 99.93 and H, 0. Freestanding carbon and graphite films were obtained from the iodine-doped PA films through carbonization at 800 °C followed by graphitization at 1400−3000 °C.

2.6. Morphologies of Carbon and Graphite Films. Importantly, the fibril morphology of the typical PA film remained unchanged after the carbonization at 800 °C, as indicated in the SEM image of the carbon film (Figure S2a in the Supporting Information). A morphology consisting of entangled fibrils was observed in the carbon film prepared from a fully doped typical PA film. Note that the carbon film prepared from the less-doped PA film ($[CHI_{0.07}]_n$) retained neither a fibril morphology nor the original film shape after the carbonization (Figure S3 in the Supporting Information). By contrast, an aligned morphology was observed in the carbon film prepared from the stretched PA film ($[CHI_{0.33}]_n$) after the morphology-retaining carbonization (Figure S2e in the Supporting Information).

Figure 5 presents photographs of the S-type, unstretched, and stretched PA films graphitized at 2600 °C. Notably, the graphite film prepared through a heat treatment at 2600−3000 °C has almost the same surface morphology and film shape as that of the original PA film and as that of the carbon film prepared at 800 °C, even in the aligned graphite film prepared from the stretched PA film [Figures 5 and S4 (Supporting Information)]. The surface of the gas side of the typical PA film graphitized at 2600 °C exhibited a more porous morphology than that of the glass side in SEM images [Figures 5b and S5c (Supporting Information)]. The porosity (P) of the graphite film was estimated to be 39−53% using the following equation: P (%) = 100[1 − (d_{bulk}/d_{true})], where d_{bulk} is the bulk density of the film and d_{true} is the true density of graphite (2.25 g/cm^3).

2.7. XRD Patterns of Carbon and Graphite Films. The XRD patterns of the carbon films prepared at 800 °C present no crystalline reflections (Figure S6 in the Supporting Information), implying that the films exist in an amorphous state. Figure 6 presents XRD patterns of the typical PA films

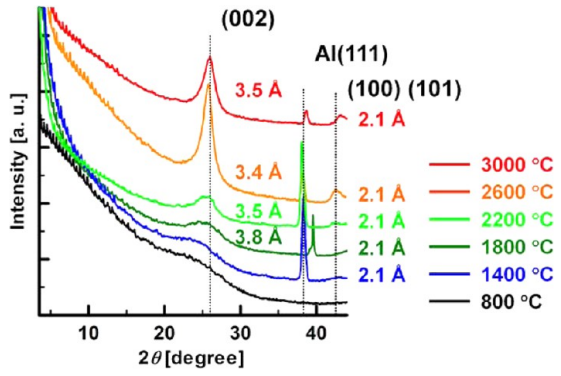

Figure 6. XRD patterns of the carbon films prepared from the typical PA films ($[CHI_{0.24-0.26}]_n$) at various temperatures. The incident X-rays are perpendicular to the film surface.

carbonized at 800−3000 °C. The XRD peak corresponding to the (002) plane and the mixed reflection of (100) and (101) planes of a graphitic crystal essentially increased with increasing heat-treatment temperature,[26] indicating that the number of graphite layers in the crystalline structures, the degree of crystallinity, and the crystal sizes are supposed to increase with increasing heat-treatment temperature. In particular, the sharp (002) peak of the graphite film prepared at 2600 °C indicates that the graphitic crystallization proceeds in the carbon film through the heat treatment. The crystal size along the c-axis

DOI: 10.1021/jacs.5b04012
J. Am. Chem. Soc. 2015, 137, 9077−9087

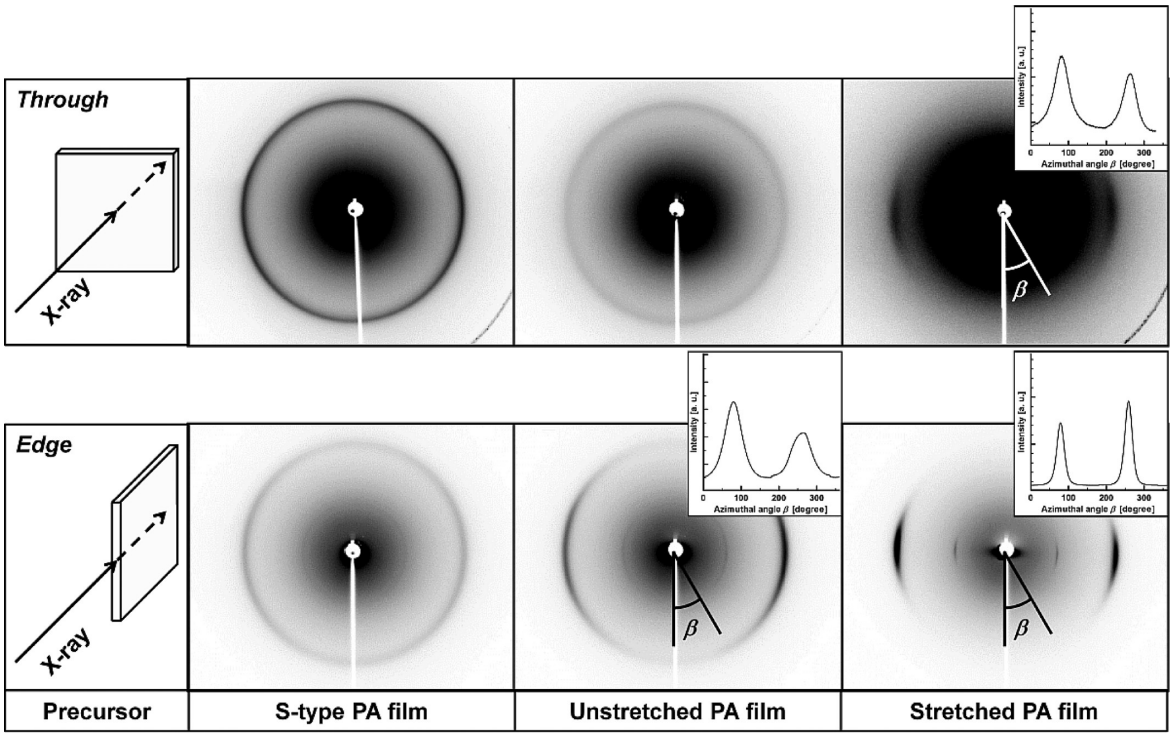

Figure 7. Laue XRD patterns of the S-type (left), unstretched (middle), and stretched (right) PA films graphitized at 2600 °C. The insets present the azimuthal-angle profiles based on the (002) reflection of the XRD pattern.

(L_c) of the graphite film was estimated to be approximately 4.7 nm from the (002) plane of the powder XRD pattern (Figure S7c in Supporting Information). The present graphite film is found to possess, on average, 14 graphite layers in the crystalline structure based on the d_{002}-spacing and the L_c. Using these parameters of the carbonaceous materials, the d_{002}-spacing is estimated to be close to the theoretical value of 3.35 Å.

Figure 7 presents Laue XRD patterns in the through and edge directions of the S-type, unstretched, and stretched PA films graphitized at 2600 °C. To investigate the degree of in-plane orientation of the graphitic crystallites in the graphite film, the intensity ratio of the (002) plane and (100) (101) planes ($I_{002}/I_{100\,101}$) was estimated from the XRD pattern. The structural parameters of the graphite films are summarized in Table S1 of the Supporting Information. The XRD patterns in the through and edge directions of the typical PA film graphitized at 2600 °C show $I_{002}/I_{100\,101}$ ratios of 9.0 and 16 (Figure S7a,b in the Supporting Information), respectively, indicating that the film is composed of almost randomly arranged graphitic crystallites with no specific orientation. This result is in good agreement with the randomly arranged fibril morphology of the film (Figure 5b). In contrast, the XRD pattern in the edge direction of the stretchable PA film graphitized at 2600 °C shows a considerably larger $I_{002}/I_{100\,101}$ ratio than that in the through direction (Figures S8 and S9 in the Supporting Information), indicating that the graphene layers tend to be parallel to the film surface. The aligned XRD patterns in the edge direction of the graphite film also clearly show the in-plane orientation of the layers in the film (Figure 7). The graphite film prepared from the stretched PA film shows a higher degree of in-plane orientation than that from the unstretched one because the former has a higher orientation factor than the latter. Note that such an orientation in the graphite film is similar to the case of PPV (poly-*p*-phenylenevinylene)-based graphite films.[27] Furthermore, the stretched PA film afforded a graphite film with a higher crystallinity and a distinct crystal size. The L_c values of the graphite films prepared from the unstretched and stretched PA films were estimated to be approximately 5.3 and 11 nm from the (002) planes of powder XRD patterns, respectively (Figures S8c and S9c in the Supporting Information). The present graphite films are found to possess, on average, 16 and 31 graphite layers in the crystalline structure based on the d_{002}-spacing and the L_c, respectively.

The stretched PA film graphitized at 2600 °C exhibited an aligned XRD pattern not only in the edge direction but also in the through direction. The equatorial reflection was determined to be 3.4−3.5 Å, and therefore, it corresponds to an interlayer distance in the graphitic crystal. This reflection can be assigned as the distance between graphene layers macroscopically aligned parallel to the direction of stretching. This is because the PA chains aligned parallel to the direction of stretching effectively cross-link each other during the heating process and because the graphenes formed from the cross-linked polyene chains closely stack, yielding graphite structures along the direction parallel to the alignment. The orientation factor of the graphite film was calculated to be 0.28−0.33 in the through direction and 0.77 in the edge direction. These values are lower than those of the original PA film after the stretching treatment. The difference in the degree of orientation between the aligned PA and graphite films is due to thermal shrinkage during the heat treatment, particularly during the carbonization process, and the disordering in the molecular structure arrangement during the thermal transformation from polymer chains to a graphene-like structure.

2.8. Raman Scattering Spectra of PA, Carbon, and Graphite Films. The Raman scattering spectrum of the typical

DOI: 10.1021/jacs.5b04012
J. Am. Chem. Soc. 2015, 137, 9077−9087

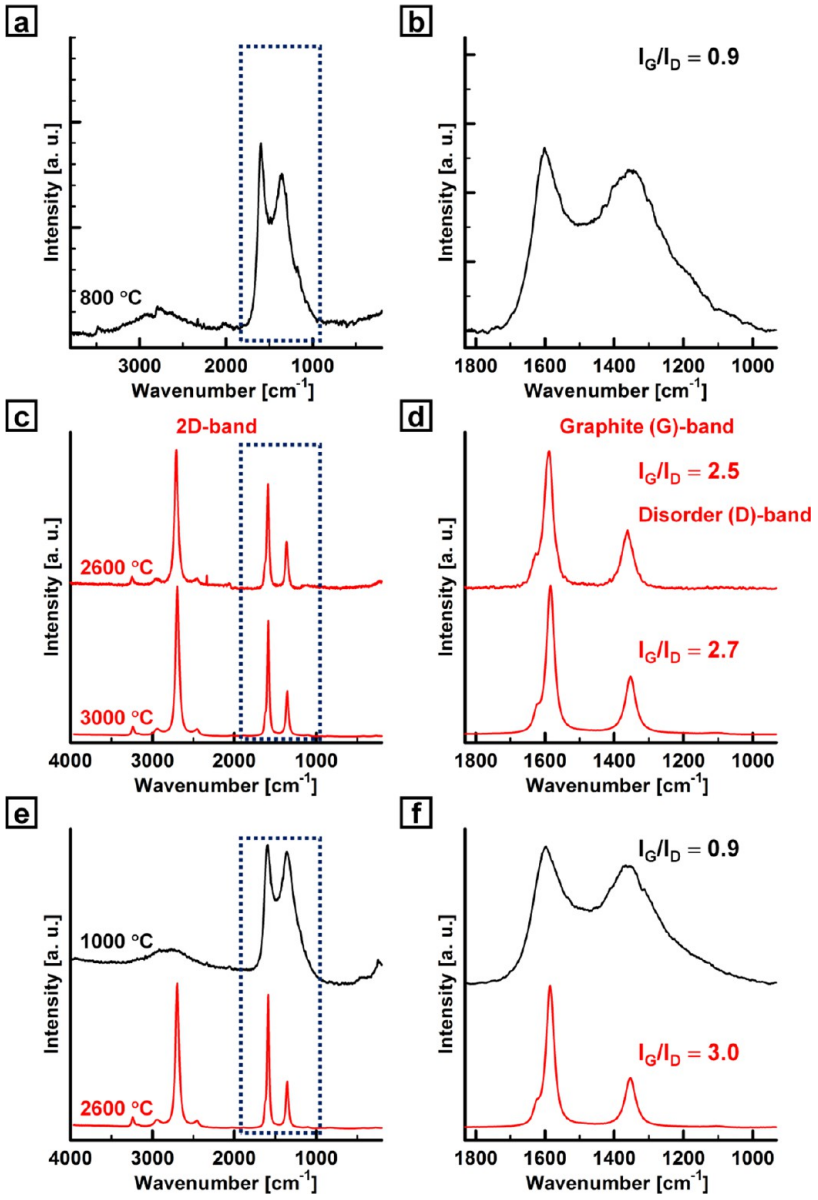

Figure 8. Raman scattering spectra of the carbon (black) and graphite (red) films prepared from the (a, c) S-type and (e) stretchable PA films and (b, d, f) their magnified spectra.

PA film presents two large bands at approximately 1494 and 1119 cm^{-1}, which are assigned to the C=C stretching vibration and the mixed vibration of C−C stretching and C−H in-plane bending of *trans*-PA, respectively (Figure S10 in Supporting Information).[28] The Raman spectrum of the typical PA film carbonized at 800 °C presents a broad disorder band (D-band) at 1357 cm^{-1} and a strong graphite band (G-band) at 1601 cm^{-1} (Figure 8a,b). The D- and G-bands decrease and increase in intensity, respectively, and the two bands become sharp, after the graphitization at 2600−3000 °C (Figure 8d). The sharp Raman band observed at 2696−2708 cm^{-1} in the graphite film is assigned to the so-called 2D-band, which is often observed in graphitic materials (Figure 8c).[29] The crystal sizes along the *a*-axis (L_a) of the carbon and graphite films were estimated from the Raman spectra to be 3.8 and 8.0−8.7 nm, respectively. The L_a of the typical PA film graphitized at 3000 °C is slightly larger than that of the PA film graphitized at 2600 °C. The Raman spectrum of the stretchable PA film carbonized at 1000 °C shows a D-band at 1366 cm^{-1} and a G-band at 1598 cm^{-1} (Figure 8e,f). The L_a of the carbon and graphite films prepared from the stretchable PA film was estimated to be 4.1 and 9.6 nm, respectively. Among the graphite films, the stretched PA film graphitized at 2600 °C has the highest L_a, which is in agreement with the result of the XRD profile.

From the results of XRD patterns and Raman spectra, graphite films with a higher degree of crystallinity are obtained when using the stretched PA films as precursors. However, their crystallinity is still not enough when compared with polyimide (PI)-based graphite films and polyacrylonitrile (PAN)-based graphite fibers because the D-band is still pronounced in the Raman spectra, even after the heat treatment up to 3000 °C. This lack of crystallinity is rationalized as follows: it is well-known that the inherently rigid backbone of aromatic PI derivatives is easily graphitized, and highly crystalline graphite fibers are produced through an aromatization step followed by carbonization and graphitization processes. It is considered that the aromatic units in the precursor polymer structure facilitate positive effects for the formation of graphite crystal. In contrast,

DOI: 10.1021/jacs.5b04012
J. Am. Chem. Soc. 2015, 137, 9077−9087

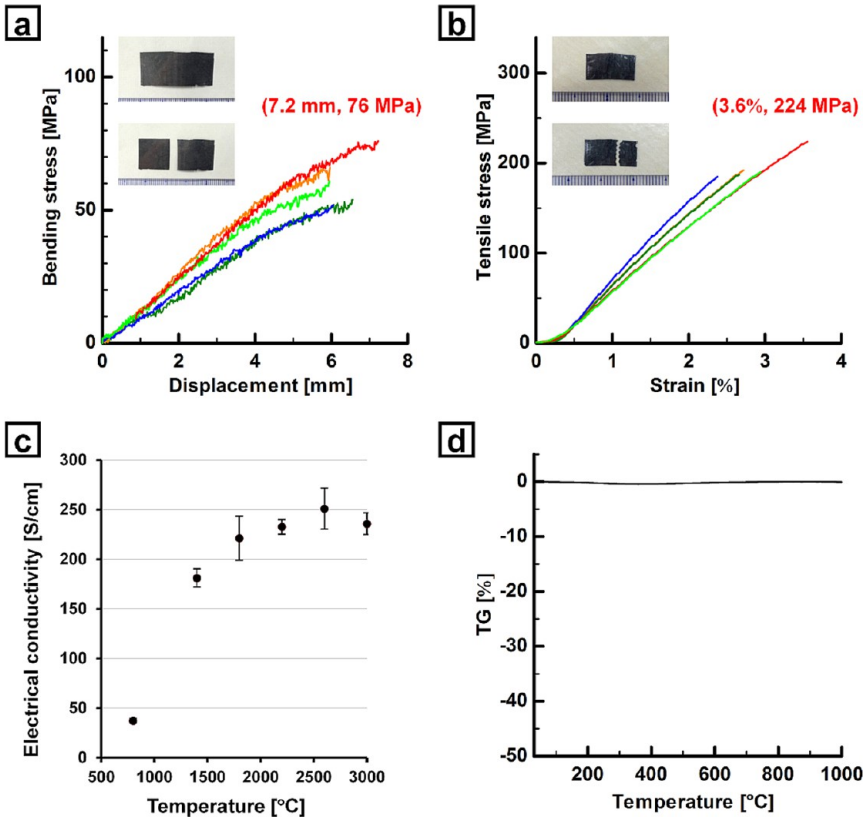

Figure 9. (a) The stress−displacement curves for five different measurements during the three-point bending test of the graphite film (t = 60 ± 11 μm) prepared from the typical PA film [$(CHI_{0.17})_n$] at 2600 °C. (b) The stress−strain curves for five different measurements during the tensile test of the graphite film (t = 55 ± 6 μm) prepared from the typical PA film [$(CHI_{0.27})_n$] at 2600 °C. The insets present photographs of the graphite film before (upper) and after (lower) the measurement. (c) Electrical conductivity of the carbon films (t = 52−82 μm) prepared from the typical PA films ($[CHI_{0.24-0.30}]_n$) as a function of heat-treatment temperature. The error bars represent the standard deviation from several measurements. (d) TG curve of the typical PA film ($[CHI_{0.22}]_n$) graphitized at 2600 °C, indicating the high thermal stability of the film (weight loss <0.5% up to 1000 °C).

aliphatic PAs have no such aromatic units in their molecular structure. Therefore, PA films could possess a fundamental difficulty to be completely graphitized that is related to the intrinsic chemistry itself.

2.9. Mechanical Properties of Graphite Films. The mechanical properties of the typical PA film graphitized at 2600 °C were evaluated through tensile and three-point bending tests at room temperature. The average bending strength and modulus of the graphite film were 62 ± 10 MPa ($\sigma_{b,max}$ = 76 MPa, $\sigma_{b,min}$ = 52 MPa) and 16 ± 3 GPa ($\varepsilon_{b,max}$ = 19 GPa, $\varepsilon_{b,min}$ = 12 GPa), respectively (Figure 9a), which are both comparable to those of CNT blocks and are both higher than those of commercial graphites.[30] The graphite film has a higher bending flexibility than the stretchable PA film graphitized at 2600 °C because of its entangled fibril morphology. In contrast, the average tensile strength and modulus of the graphite film were 196 ± 16 MPa ($\sigma_{t,max}$ = 224 MPa, $\sigma_{t,min}$ = 185 MPa) and 8 ± 1 GPa ($\varepsilon_{t,max}$ = 10 GPa, $\varepsilon_{t,min}$ = 7 GPa), respectively (Figure 9b). This strength is higher than that of the previously reported graphite foils,[1] buckypapers,[31,32] graphene papers,[3d,33] and graphene oxide papers[3a,d] and is slightly lower than the highest value of graphene papers reported by Chen et al.[3c] The tensile property of the graphite film was higher than that of the corresponding film carbonized at 800 °C. The average tensile strength and modulus of the carbon film were 66 ± 16 MPa ($\sigma_{t,max}$ = 81 MPa, $\sigma_{t,min}$ = 45 MPa) and 6 ± 2 GPa ($\varepsilon_{t,max}$ = 9 GPa, $\varepsilon_{t,min}$ = 4 GPa), respectively (Figure S11a in Supporting Information). This difference in mechanical properties between the carbon and graphite films can be rationalized as follows: the graphite film has a larger graphitic crystalline structure with a significant crystal size in a carbon fibril than the amorphous carbon film, leading to the enhancement in the strength and modulus through the heat treatment at 2600 °C. Furthermore, although the graphite film prepared from the stretchable PA film exhibited a lower tensile strength than that from the typical PA film, the former showed a higher tensile modulus than the latter. This is probably due to the tightly entangled fibril structure of the graphite film prepared from the typical PA film, leading to the higher tensile strength than that from the stretchable PA film. The highest tensile strength and modulus of the graphite film prepared from the stretched PA film at 2600 °C were 126 MPa and 22 GPa, respectively (Figure S11b in Supporting Information).

2.10. Electrical Conductivities of Carbon and Graphite Films. The electrical conductivities of the iodine-doped PA, carbon, and graphite films were roughly measured using the four-point probe method at room temperature. The film carbonized at 800 °C and the film graphitized at 2600 °C prepared from the fully doped typical PA film have conductivities of 37 ± 2 S/cm (t = 82 ± 1 μm) and 251 ± 21 S/cm (t = 52 ± 1 μm), respectively (Figure 9c). The graphite film prepared from the less-doped typical PA film exhibited a higher conductivity than that from the fully doped film due to its dense surface morphology (Figure S3 in the Supporting Information). The carbon and graphite films prepared from the unstretched PA film exhibited conductivities

DOI: 10.1021/jacs.5b04012
J. Am. Chem. Soc. 2015, 137, 9077−9087

of 58 ± 5 S/cm (t = 45 ± 9 μm) and 282 ± 33 S/cm (t = 46 ± 8 μm), respectively. Note that the conductivity of the present graphite film is higher than that of the PA-based helical graphite film (σ on the order of 100 S/cm),[7a,b] even in a relatively thick film. This result is probably due to the difference in bulk density between the present graphite film and the helical one. Although the present graphite film is considerably lighter than bulk graphites due to its high porosity, it has a higher bulk density of 1.05−1.61 g/cm^3 than that of the helical graphite film (<1.00 g/cm^3), leading to the relatively high conductivity.

The conductivity of the graphite films increased through chemical doping with fuming nitric acid (HNO_3). The HNO_3 doping was performed by immersing the graphite film in fuming HNO_3 in a glass vial at room temperature for over 24 h. The doped graphite film retained its morphology throughout the doping (Figure S12a in the Supporting Information). Figure S12b in the Supporting Information presents a typical IR absorption spectrum of the graphite nitrate film. The absorption band at 1385 cm^{-1} provides evidence that a NO_3^- ion is formed as a dopant species in the graphite film.[34] Furthermore, the graphite film prepared from the stretched PA film exhibits an increase in conductivity compared with the unstretched film. The maximum conductivity parallel to the stretching direction ($\sigma_\parallel$) in the relatively thin film was determined to be 1501 ± 194 S/cm (t = 4 ± 2 μm). This is approximately 5−6 times higher than the conductivity of the S-type and unstretched PA films graphitized at 2600 °C. The main benefit of stretching the PA film is the enhancement in the electrical property of the graphite film. The aligned graphite film also exhibited an electrical anisotropy in which the conductivity parallel to the direction of stretching was higher than that perpendicular to the direction. This anisotropy, defined as the parallel-to-perpendicular value of the conductivity ($\sigma_\parallel/\sigma_\perp$), ranged from 1.1−1.3, depending on the sample. The unexpectedly lower value is attributed to the formation of networks of sp^2 hexagonal carbon bonds during the heat treatment via a thermal cross-linking between the adjacent PA chains, which produce diagonal transportation passes of charged carriers and enhance the perpendicular conductivity.

3. CONCLUSIONS

It was demonstrated that an iodine-doped PA film is a highly efficient carbon source for producing graphite films with good mechanical and electrical properties. The present carbonization procedure provides a graphite film with a total yield as high as 61−74% at up to 3000 °C, which is considerably higher than that of PAN-based carbon fiber (up to 56%)[35] and PI-based graphite film (50−55%)[36,37] and is slightly lower than the carbonization yield of pitch-based carbon fiber (80−85%).[38,39] Furthermore, the highly mechanically stretched PA film retained its aligned morphology even after the carbonization and subsequent graphitization, affording an anisotropic graphite film with enhanced conductivity. We expect that the strong, electrically conductive, thermally stable, and single-component graphite films might exhibit unique functional properties that are characteristic of the entangled fibril morphology or anisotropic structure and could also be used as a porous carbon paper suitable for a gas diffusion layer in polymer electrolyte fuel cells or as an anisotropic carbon negative electrode material for lithium ion batteries. We plan to perform such experiments for one of the particular applications, and the details will be reported in the near future.

■ ASSOCIATED CONTENT

Supporting Information

Materials and measurements, acetylene polymerizations, electrical conductivity and stability as a function of stretching degree, Figures S1−S20, and Tables S1−3. The Supporting Information is available free of charge on the ACS Publications website at DOI: 10.1021/jacs.5b04012.

■ AUTHOR INFORMATION

Corresponding Author

*akagi@fps.polym.kyoto-u.ac.jp

Notes

The authors declare no competing financial interest.

■ ACKNOWLEDGMENTS

We thank Dr. A. Kaito and Dr. M. Shimomura (AIST, Japan) and JASCO Co., Ltd. for the measurements of Raman spectra, and Dr. S. Ohshima and Dr. T. Saito (AIST, Japan) for the use of the graphitizing apparatus (Sanriko denki). We thank Nippon Paper Industries Co., Ltd. for the use of the graphitizing apparatus [SCC-U-80/150 (2P), Kurata Giken]. The authors are grateful to Dr. M. Kyotani (University of Tsukuba, Japan) for his helpful cooperation and support. The authors are also grateful to Mr. A. Yagi (DENKA) and to laboratory colleagues Ms. B. Yan, Mr. T. Uchida, Mr. K. Nishino, and Mr. H. Horikawa, Department of Polymer Chemistry, Kyoto University, for their helpful cooperation and support in synthesizing PA films. This work was supported by a Grant-in-Aid for Scientific Research (A) (No. 13370214) and that for Young Scientists (B) (No. 24750219) from the Ministry of Education, Culture, Sports, Science and Technology, Japan.

■ REFERENCES

(1) (a) Dowell, M. B.; Howard, R. A. *Carbon* **1986**, *24*, 311−323. (b) Leng, Y.; Gu, J.; Cao, W.; Zhang, T.-Y. *Carbon* **1998**, *36*, 875−881.

(2) (a) Liu, J.; Rinzler, A. G.; Dai, H.; Hafner, J. H.; Bradley, R. K.; Boul, P. J.; Lu, A.; Iverson, T.; Shemimov, K.; Huffman, C. B.; Rodriguez-Macias, F.; Shon, Y.-S.; Lee, T. R.; Colbert, D. T.; Smalley, R. E. *Science* **1998**, *280*, 1253−1256. (b) Liu, L.; Ma, W.; Zhang, Z. *Small* **2011**, *7*, 1504−1520.

(3) (a) Dikin, D. A.; Stankovich, S.; Zimney, E. J.; Piner, R. D.; Dommett, G. H. B.; Evmenenko, G.; Nguyen, S. T.; Ruoff, R. S. *Nature* **2007**, *448*, 457−460. (b) Li, D.; Müller, M. B.; Gilje, S.; Kaner, R. B.; Wallace, G. G. *Nat. Nanotechnol.* **2007**, *3*, 101−105. (c) Chen, H.; Müller, M. B.; Gilmore, K. J.; Wallace, G. G.; Li, D. *Adv. Mater.* **2008**, *20*, 3557−3561. (d) Compton, O. C.; Nguyen, S. T. *Small* **2010**, *6*, 711−723.

(4) (a) Zhang, M.; Fang, S.; Zakhidov, A. A.; Lee, S. B.; Aliv, A. E.; Williams, C. D.; Atkinson, K. R.; Baughman, R. H. *Science* **2005**, *309*, 1215−1219. (b) Yamada, T.; Namai, T.; Hata, K.; Futaba, D. N.; Mizuno, K.; Fan, J.; Yudasaka, M.; Yumura, M.; Iijima, S. *Nat. Nanotechnol.* **2006**, *1*, 131−136. (c) Ci, L.; Manikoth, S. M.; Li, X.; Vajtai, R.; Ajayan, P. M. *Adv. Mater.* **2007**, *19*, 3300−3303.

(5) (a) Cai, J.; Ruffieux, P.; Jaafar, R.; Bieri, M.; Braun, T.; Blankenburg, S.; Muoth, M.; Seitsonen, A. P.; Saleh, M.; Feng, X.; Müllen, K.; Fasel, R. *Nature* **2010**, *466*, 470−473. (b) Liu, R.; Wu, D.; Feng, X.; Müllen, K. *J. Am. Chem. Soc.* **2011**, *133*, 15221−15223. (c) Yang, S.; Bachman, R.; Feng, X.; Müllen, K. *Acc. Chem. Res.* **2013**, *46*, 116−128.

(6) Sokolov, A. N.; Yap, F. L.; Liu, N.; Kim, K.; Ci, L.; Johnson, O. B.; Wang, H.; Vosgueritchian, M.; Koh, A. L.; Chen, J.; Park, J.; Bao, Z. *Nat. Commun.* **2013**, *4*, 2402.

(7) (a) Kyotani, M.; Matsushita, S.; Nagai, T.; Matsui, Y.; Shimomura, M.; Kaito, A.; Akagi, K. *J. Am. Chem. Soc.* **2008**, *130*,

DOI: 10.1021/jacs.5b04012
J. Am. Chem. Soc. 2015, 137, 9077−9087

10880−10881. (b) Matsushita, S.; Kyotani, M.; Akagi, K. *J. Am. Chem. Soc.* **2011**, *133*, 17977−17992. (c) Matsushita, S.; Yan, B.; Yamamoto, S.; Jeong, Y. S.; Akagi, K. *Angew. Chem., Int. Ed.* **2014**, *53*, 1659−1663.
(8) Frank, E.; Steudle, L. M.; Ingildeev, D.; Spörl, J. M.; Buchmeiser, M. R. *Angew. Chem., Int. Ed.* **2014**, *53*, 2−39.
(9) *New Carbon: Control of Structure and Functions*; Inagaki, M., Ed.; Elsevier: Amsterdam, 2000.
(10) Yan, B.; Matsushita, S.; Suda, K.; Akagi, K. *Chem. Mater.* **2015**, *27*, 2973−2980.
(11) (a) Araya, K.; Mukoh, A.; Narahara, T.; Shirakawa, H. *Synth. Met.* **1986**, *14*, 199−206. (b) Kyotani, M.; Matsushita, S.; Goh, M.; Nagai, T.; Matsui, Y.; Akagi, K. *Nanoscale* **2010**, *2*, 509−514.
(12) (a) Akagi, K.; Katayama, S.; Shirakawa, H.; Araya, K.; Mukoh, A.; Narahara, T. *Synth. Met.* **1987**, *17*, 241−246. (b) Goh, M.; Matsushita, T.; Satake, H.; Kyotani, M.; Akagi, K. *Macromolecules* **2010**, *43*, 5943−5948.
(13) Ribet, J. L.; Rolland, M.; Montaner, A.; Galtier, M.; Lakhliai, Z.; Sauvajol, J. L.; Brunet, M.; Almairac, R.; Bernier, P. *Synth. Met.* **1988**, *24*, 1−5.
(14) (a) Naarmann, H.; Theophilou, N. *Synth. Met.* **1987**, *22*, 1−8. (b) Naarmann, H. *Synth. Met.* **1987**, *17*, 223−228.
(15) Akagi, K.; Suezaki, M.; Shirakawa, H.; Kyotani, H.; Shimomura, M.; Tanabe, Y. *Synth. Met.* **1989**, *28*, D1−D10.
(16) (a) Akagi, K.; Sakamaki, K.; Shirakawa, H. *Macromolecules* **1992**, *25*, 6725−6726. (b) Akagi, K.; Sakamaki, K.; Shirakawa, H. *Synth. Met.* **1993**, *55*−*57*, 779−784.
(17) Tsukamoto, J.; Takahashi, A.; Kawasaki, K. *Jpn. J. Appl. Phys.* **1990**, *29*, 125−130.
(18) Ito, T.; Shirakawa, H.; Ikeda, S. *J. Polym. Sci., Polym. Chem. Ed.* **1974**, *12*, 11−20.
(19) Shirakawa, H.; Ikeda, S. *Synth. Met.* **1979**/**80**, *1*, 175−184.
(20) Michl, J.; Thulstrup, E. W. *Spectroscopy with Polarized Light*; VCH: New York, 1986.
(21) Galtier, M.; Charbonnel, M.; Montaner, A.; Ribet, J. L. *Polymer* **1984**, *25*, 1253−1257.
(22) Hermans, P. H.; Platzek, P. *Kolloid-Z.* **1939**, *88*, 68−72.
(23) Ito, T.; Shirakawa, H.; Ikeda, S. *J. Polym. Sci., Polym. Chem. Ed.* **1975**, *13*, 1943−1950.
(24) Chien, J. C. W.; Uden, P. C.; Fan, J. *J. Polym. Sci.: Polym. Chem. Ed.* **1982**, *20*, 2159−2167.
(25) The determination of the oxygen content of the carbon film by EA was analytically difficult because of the incombustibility of the film at up to 1090 °C.
(26) Kyotani, M.; Matsushita, S.; Kimura, S.; Akagi, K. *J. Anal. Appl. Pyrolysis* **2012**, *95*, 14−20.
(27) Ohnishi, T.; Murase, I.; Noguchi, T.; Hirooka, M. *Synth. Met.* **1986**, *14*, 207−213.
(28) Arbuckle, G. A.; Buecheler, N. M.; Hall, J. W.; Valentine, K. G.; Lefrant, S.; Mevellec, J. Y.; Mulazzi, E. *Synth. Met.* **1996**, *79*, 183−188.
(29) Pimenta, M. A.; Dresselhaus, G.; Dresselhaus, M. S.; Cançado, L. G.; Jorio, A.; Saito, R. *Phys. Chem. Chem. Phys.* **2007**, *9*, 1276−1291.
(30) Sato, Y.; Ootsubo, M.; Yamamoto, G.; Van Lier, G.; Terrones, M.; Hashiguchi, S.; Kimura, H.; Okubo, A.; Motomiya, K.; Jeyadevan, B.; Hashida, T.; Tohji, K. *ACS Nano* **2008**, *2*, 348−356.
(31) (a) Zhang, X.; Sreekumar, T. V.; Liu, T.; Kumar, S. *J. Phys. Chem. B* **2004**, *108*, 16435−16440. (b) Kumar, N. A.; Jeon, I.-Y.; Sohn, G.-J.; Jain, R.; Kumar, S.; Baek, J.-B. *ACS Nano* **2011**, *5*, 2324−2331.
(32) Dettlaff-Weglikowska, U.; Skákalova, V.; Graupner, R.; Jhang, S. H.; Kim, B. H.; Lee, H. J.; Ley, L.; Park, Y. W.; Berber, S.; Tománek, D.; Roth, S. *J. Am. Chem. Soc.* **2005**, *127*, 5125−5131.
(33) Xin, G.; Sun, H.; Hu, T.; Fard, H. R.; Sun, X.; Koratkar, N.; Borca-Tasciuc, T.; Lian, J. *Adv. Mater.* **2014**, *26*, 4521−4526.
(34) *Infrared and Raman Spectra of Inorganic and Coordination Compounds*, 4th ed.; Nakamoto, K., Ed.; John Wiley & Sons: New York, 1986.
(35) Nataraj, S. K.; Yang, K. S.; Aminabhavi, T. M. *Prog. Polym. Sci.* **2012**, *37*, 487−513.
(36) Bürger, A.; Fitzer, E.; Heym, M.; Terwiesch, B. *Carbon* **1975**, *13*, 149−157.
(37) Inagaki, M.; Ohta, N.; Hishiyama, Y. *Carbon* **2013**, *61*, 1−21.
(38) Otani, S. *Carbon* **1965**, *3*, 31−38.
(39) Matsumoto, T. *Pure Appl. Chem.* **1985**, *57*, 1553−1562.

DOI: 10.1021/jacs.5b04012
J. Am. Chem. Soc. 2015, 137, 9077−9087